

Spin-orbit coupled two-electron Fermi gases of ytterbium atoms

Bo Song,¹ Chengdong He,¹ Shanchao Zhang,¹ Yueyang Zou,¹ Elnur Hajiyev,¹ Wei Huang,^{1,*} Xiong-Jun Liu,² and Gyu-Boong Jo¹

¹*Department of Physics, The Hong Kong University of Science and Technology, Clear Water Bay, Kowloon, Hong Kong, China*

²*International Center for Quantum Materials, School of Physics, Peking University, Beijing, China*

We demonstrate the spin-orbit coupling (SOC) in a two-electron Fermi gas of ^{173}Yb atoms by coupling two hyperfine ground states via the two-photon Raman transition. Due to the $\text{SU}(N)$ symmetry of the $^1\text{S}_0$ ground-state manifold which is insensitive to external magnetic field, an optical AC Stark effect is applied to split the ground spin states and separate an effective spin-1/2 subspace out from other hyperfine levels for the realization of SOC. With a momentum-dependent spin-orbit gap being suddenly opened by switching on the Raman transition, the dephasing of spin dynamics is observed, as a consequence of the momentum-dependent Rabi oscillations. Moreover, the momentum asymmetry of the spin-orbit coupled Fermi gas is also examined after projection onto the bare spin state and the corresponding momentum distribution is measured for different two-photon detuning. The realization of SOC for Yb fermions may open a new avenue to the study of novel spin-orbit physics with alkaline-earth-like atoms.

Ultracold atoms are fascinating for the study of synthetic quantum system which is direct analogy to real electronic material [1]. One of the notable examples is the implementation of synthetic gauge field and spin-orbit coupling (SOC) engineered with the atom-light interaction at will [2, 3]. In particular, SOC links a particle's spin with its momentum, which is not only essential in novel quantum phenomena, such as spintronic effect [4] and exotic topological states of quantum matter [5, 6], but also provides an unprecedented quantum system such as spin-half spin-orbit coupled bosons without analogy in condensed matter [7]. Various types of SOC can be generated in ultracold atoms where the relevant parameters are tunable through changing the laser fields [8–10] or the magnetic field [11]. So far, the SOC along the one direction have been created in bosonic [7, 12–19], fermionic alkali atoms [20–23], and very recently in fermionic lanthanide atoms [24]. Besides the 1D SOC, the two-dimensional synthetic SOC were also created both in the bosonic and fermionic atoms [25, 26].

The optical Raman transition is a common way to couple different internal states transferring momentum to the atoms [2, 3]. In alkali atoms, due to the small fine-structure splitting of the excited level, these processes inevitably suffer from heating effect caused by spontaneous emission. This could limit the ability to observe interacting many-body phenomena that needs long timescales. Recently to avoid such heating, the specific atomic species with large ground-state angular momentum such as Dy have been considered [27, 28] or the external orbital states, representing pseudo-spins, in optical superlattices have been used to generate SOC [29].

Recent development of alkaline-earth-like atoms has led to an increasing potential in utilizing such atoms not only for the study of many-body physics [30–33] but also for the realization of synthetic gauge field in a Fermi

gas [34, 35]. The narrow optical transition of alkaline-earth atoms and the large fine-structure splitting, for example, may allow to alleviate spontaneous heating when SOC is generated. Interestingly, its ground state is insensitive to the magnetic field unlike the alkali or lanthanide atoms. In the SOC experiment of ^{173}Yb , for example, one does not need to provide extreme magnetic field stability in order to precisely control the two-photon detuning. Furthermore, the alkaline-earth-like atom with large nuclear spins offers a new possibility to realize spin-orbit coupled high spin fermions [3] like a spin-1 bosonic gas with SOC [36], intriguing magnetic crystals [37] and atomic simulator of $U(N)$ and $\text{SU}(N)$ lattice gauge theories [38].

Here, we implement spin-orbit coupling in a two-electron degenerate Fermi gas of ^{173}Yb atoms by using the two-photon optical Raman transition. The dephasing spin dynamics during the Rabi oscillation and the asymmetric momentum distribution of the spin-orbit coupled Fermi gas are observed as a hallmark of SOC. In contrast to spin-orbit-coupled alkali or lanthanides fermionic atoms, here the two-photon detuning is controlled by the light-induced AC shift for ^{173}Yb atoms without suffering from additional heating caused by the magnetic field fluctuation.

Implementation of SOC in an ytterbium gas We generate spin-orbit coupling in a Fermi gas of ^{173}Yb atoms by the use of the intercombination $\lambda_0=556$ nm transition connecting two hyperfine levels with the Raman transition [22, 23]. A pair of Raman coupling beams, intersecting at $\theta=90^\circ$, are red-detuned by ~ 1 GHz from the $^1\text{S}_0(F=\frac{5}{2}) \leftrightarrow ^3\text{P}_1(F'=\frac{7}{2})$ narrow linewidth transition. The $F=\frac{5}{2}$ ground-state manifold has six hyperfine levels with magnetic sublevels $|m_F| \leq \frac{5}{2}$ that are typically degenerate due to their small magnetic moment which entirely stems from the nuclear spin.

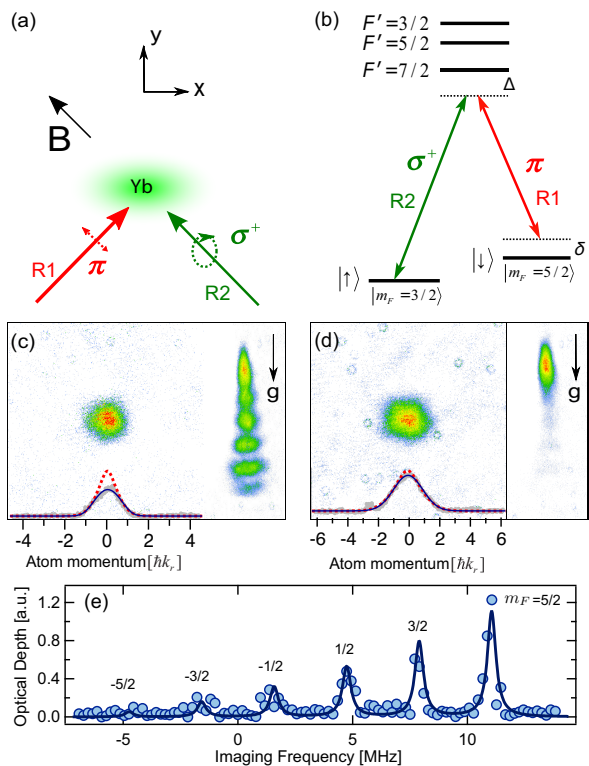


FIG. 1. (color online) Schematic diagram of the Raman transition configuration. (a) A single-component fermi gas of ^{173}Yb atoms is prepared with bias magnetic field along the $(-\hat{x} + \hat{y})$ direction and exposed to a pair of two 556 nm Raman beams (linearly polarized along $(-\hat{x} + \hat{y})$ and circularly polarized respectively) at 45° relative to \hat{y} axis. (b) A pair of Raman beams couples two ground-state hyperfine level with the single-photon detuning $\Delta = 1$ GHz from the excited state $F' = \frac{7}{2}$. (c) A six-component Fermi gas of ^{173}Yb atoms with $N = 5.0 \times 10^4$ is obtained at $T/T_F \leq 0.27$. A time-of-flight image is obtained after 11 ms free expansion using the 399 nm $^1\text{S}_0 - ^1\text{P}_1$ transition. Each spin state $|m_F\rangle$ is spatially separated by the OSG light followed by 399 nm absorption imaging. (d) With optical pumping during the evaporative cooling, a single-component Fermi gas in $|m_F = \frac{5}{2}\rangle$ is cooled down to $T/T_F \simeq 0.5$ with $N = 1.2 \times 10^4$. (e) Using the $^1\text{S}_0 - ^3\text{P}_1$ intercombination line, m_F -states are resolved. The spectrum of ^{173}Yb atoms with homogeneous m_F distribution is obtained by a σ^+ -polarized light in the 5 G bias field along the imaging axis. The black solid curve indicates the expected relative line strength of the transition.

Raman process couples two hyperfine levels $|F = \frac{5}{2}, m_F = \frac{3}{2}\rangle$ and $|F = \frac{5}{2}, m_F = \frac{5}{2}\rangle$ in the $^1\text{S}_0$ ground state, labeled as spin-up $|\uparrow\rangle$ and spin-down $|\downarrow\rangle$ respectively, by imparting momentum $2\hbar k_r$ to atoms where the recoil momentum is $k_r = k_0 \sin(\theta/2)$ for $k_0 = 2\pi/\lambda_0$ and m is the mass of ytterbium atom. Each of Raman beams induces the spin-dependent AC Stark shift splitting the magnetic sublevels. We achieve the Hamiltonian that describes effective 1D SOC, with equal strengths of Rashba and Dresselhaus SOC, along the \hat{x} -direction as the pre-

vious work [7, 22, 23, 39]: $H_{\text{SOC}} = \frac{1}{2m}(p_x + k_r \sigma_z)^2 + \frac{\Omega_R}{2} \sigma_x + \frac{\delta}{2} \sigma_z$ where σ_i are Pauli matrices, p_x is the quasi-momentum of atoms along \hat{x} -direction, Ω_R is the Rabi frequency of Raman coupling and δ is the two-photon detuning. In contrast to alkali or lanthanide atoms, we tune the two-photon detuning δ using spin-dependent light shift induced by Raman beams. We independently calibrate spin-dependent level shift from different lights by monitoring the two-photon Rabi oscillation induced by a pair of co-propagating Raman beams (see appendix).

Preparation of the ytterbium gas We first prepare an ultracold Fermi gas of ^{173}Yb atoms by loading atoms, precooled by the intercombination magneto-optical trap (MOT), into the a 1064 nm crossed optical dipole trap (ODT) for forced evaporation. After the final stage of the optical evaporative cooling, we achieve a six-component degenerate Fermi gas of $\sim 5.0 \times 10^4$ atoms at $T/T_F \leq 0.27$ where T_F is the Fermi temperature of the trapped atom with the trapping frequency of $\bar{\omega} = (\omega_x \omega_y \omega_z)^{\frac{1}{3}} = 2\pi \times 130$ Hz. In this case, all six hyperfine states $|m_F = -\frac{5}{2}, -\frac{3}{2}, \dots, \frac{5}{2}\rangle$ are degenerate protected by SU(6) symmetry.

A single-component degenerate Fermi gas is then obtained using the similar optical evaporative cooling process with different initial spin configuration. We optically pump more than 70% atoms into the $|m_F = \frac{5}{2}\rangle$ state at the beginning of the evaporative cooling using the nearly resonant 556 nm light with σ^+ polarization. Note that we keep tiny fraction of $|m_F = \frac{3}{2}\rangle$ state atoms until the end of the evaporation in order to enhance the evaporative cooling. Finally, we prepare a Fermi gas of $N = 1.3 \times 10^4$ atoms in $|m_F = \frac{5}{2}\rangle$ state at $T/T_F \simeq 0.5$ together with $N = 1.0 \times 10^3$ atoms in $|m_F = \frac{3}{2}\rangle$. Additional resonant 556 nm light is applied to blast $|m_F = \frac{3}{2}\rangle$ atoms and thus obtain a pure single-component Fermi gas.

Spin-resolved detection For ytterbium isotopes, m_F -resolved absorption imaging with the broad 399 nm $^1\text{S}_0 - ^1\text{P}_1$ transition is not possible at low bias magnetic field as the Zeeman splitting of the excited $|m_{F'}\rangle$ state is not large enough compared to the natural linewidth of the transition. Here we instead use the narrow $^1\text{S}_0 - ^3\text{P}_1$ intercombination line for spin-resolved blast at the bias field of 6 G where the ground-state manifold is degenerate with SU(6) symmetry [40]. As described in Fig. 1 (e), each $|m_F\rangle$ state is spectroscopically resolved at different imaging frequency of 556 nm light following the line strength of the corresponding transition. During the time-of-flight expansion, the unwanted spin states are selectively removed with the blast light, followed by the 399 nm absorption imaging.

We also use the complimentary method to resolve different nuclear spin state by optical Stern-Gerlach (OSG) effect [40, 41]. A non-resonant circularly polarized laser beam with the beam waist of $140 \mu\text{m}$ is briefly switched on after the time-of-flight expansion starts. The spin-dependent force vertically splits the atomic cloud into six

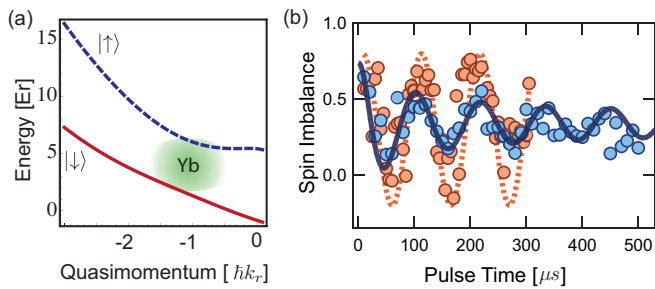


FIG. 2. (color online) Spin dynamics with spin-orbit coupling. The two-photon Rabi oscillation is monitored with the two-photon detuning of $\delta = -4.0(3)E_r$ and the Rabi frequency $\Omega_R = 4.8E_r$. (a) The single-particle energy dispersion of dressed-states. (b) The spin imbalance, defined as $(N_{|\downarrow\rangle} - N_{|\uparrow\rangle}) / (N_{|\downarrow\rangle} + N_{|\uparrow\rangle})$ for the atom number $N_{|\uparrow\rangle}$ and $N_{|\downarrow\rangle}$, is measured via 399 nm imaging together with the OSG light. The predicted spin dynamics for non-interacting fermions (blue solid curve) is consistent with the measurement (blue circle). Without SOC, the Rabi oscillation does not dephase (orange circle).

parts corresponding each $|m_F\rangle$ state as shown in Fig. 1 (c) and (d) inset.

Spin dynamics with spin-orbit coupling When two spin states $|\uparrow\rangle$ and $|\downarrow\rangle$ are coupled through the two-photon Raman transition with momentum transfer of $2k_r\hat{e}_x$, the energy gap between the dressed-states $|\uparrow'\rangle$, $\mathbf{p}_x = \mathbf{k}_x - \hbar k_r\hat{e}_x$ and $|\downarrow'\rangle$, $\mathbf{p}_x = \mathbf{k}_x + \hbar k_r\hat{e}_x$ is quasi-momentum dependent where \mathbf{p}_x denotes the quasi-momentum as shown in Fig. 2 (a). Such non-uniform spin-orbit gap induces dephasing of the spin dynamics when the Rabi oscillation is driven in a Fermi gas [22–24]. A brief pulse of Raman-coupling beams is switched on and subsequently turned off while the atoms remain in the crossed ODT. The bias magnetic field is then properly rotated to the imaging axis within 200 ms during which the nuclear spin follows the bias field adiabatically. We experimentally confirm that the spin distribution is not changed during that process owing to $SU(N)$ symmetry. Each spin state is then spatially separated by applying the OSG light followed by 4 ms time-of-flight free expansion before the 399 nm absorption imaging.

The oscillation of spin distribution is dephased as a function of pulse time which is the hallmark of the spin-orbit coupling as described in Fig. 2. In contrast, the spin dynamics is not momentum-dependent when two spin states $|\uparrow\rangle$ and $|\downarrow\rangle$ are coupled by co-propagating Raman beams that do not impart momentum transfer. The two-photon Rabi frequency Ω_R connecting $|\uparrow\rangle$ and $|\downarrow\rangle$ is then measured by fitting the oscillation of the spin population with the momentum-dependent Rabi oscillation for non-interacting fermions [22, 24] as shown in Fig. 2 (b).

Adiabatic loading into the dressed-state In order to adiabatically load atoms into the equilibrium state of

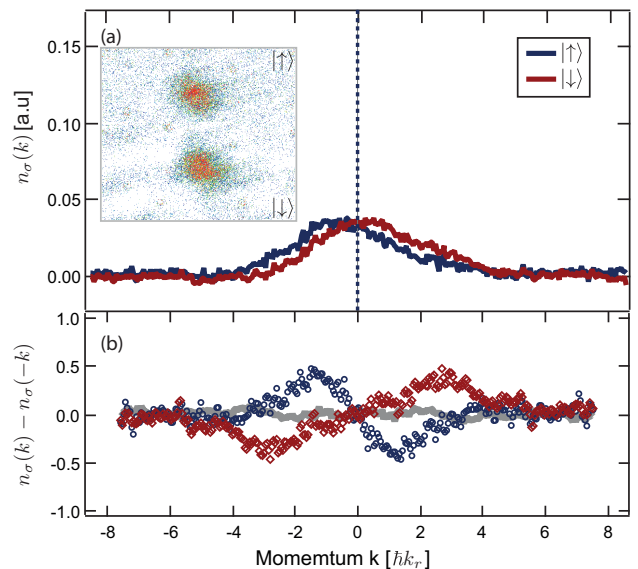


FIG. 3. (color online) Momentum distribution of a spin-orbit coupled Fermi gas of ^{173}Yb atoms. The Raman coupling with $\Omega = 1.6(3)E_r$ and $\delta = 0.1(3)$ is abruptly switched off for a gas of $N = 9 \times 10^3$ atoms followed by 399 nm absorption imaging as shown in the inset. (a) Atomic clouds after time-of-flight expansion for $|\downarrow\rangle$ and $|\uparrow\rangle$ shift in the opposite direction due to SOC. (b) The integrated momentum reveals asymmetric feature for $|\uparrow\rangle$ (blue circle) and $|\downarrow\rangle$ (red diamond) while the momentum distribution is symmetric without SOC (grey curve).

the lowest-energy dressed state [42], we start with a spin-polarized $|m_F = \frac{5}{2}, \downarrow\rangle$ Fermi gas with $T/T_F \simeq 0.5$ confined in a crossed dipole trap and adiabatically increase the Raman-coupling beam power with a 7 ms exponential ramp to the final values keeping the two-photon detuning $\delta \simeq 10E_r$ where the recoil energy is $E_r = \hbar^2 k_r^2 / 2m = 1.87$ kHz. Due to the large detuning, the atoms in the bare $|\downarrow\rangle$ state are adiabatically loaded into the dressed spin state $|\downarrow'\rangle$, by which we determine the momentum of $k_x = 0$ in the time-of-flight expansion. Subsequently, the two-photon detuning δ is exponentially ramped to the final value of detuning within 23 ms.

After adiabatic loading into the dressed state with $\Omega_R = 1.6(3)E_r$ and $\delta = 0.1(3)E_r$, we abruptly switch off the Raman beams and the crossed ODT simultaneously - thus projecting the dressed states onto the bare spin $|\uparrow, \downarrow\rangle$ and the real momentum k_x - followed by the 399 nm absorption imaging after 7 ms time-of-flight expansion with spin-selective blast 556 nm light. When the dressed energy band is symmetric for $|\uparrow\rangle$ and $|\downarrow\rangle$ at $\delta = 0.1(3)E_r$, the SOC, breaking spatial reflection symmetry, introduces asymmetric momentum distribution for bare spin states [39, 43], as highlighted in Fig. 3 where the integrated momentum distribution (blue and red curves) and $n_\sigma(k) - n_\sigma(-k)$ are plotted for spin $\sigma = \{\uparrow, \downarrow\}$. We note that such momentum asymmetry disappears if the SOC

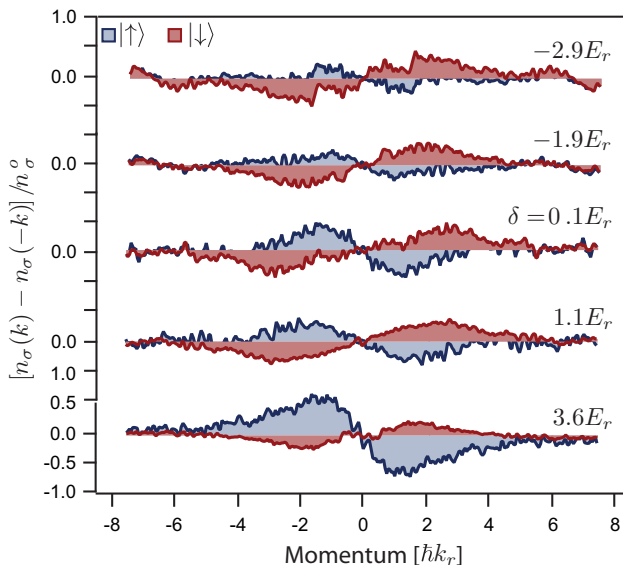


FIG. 4. (color online) Integrated momentum asymmetry along \hat{x} -direction for different values of two-photon detuning. The momentum asymmetry of the spin-orbit coupled Fermi gas is characterized by $[n_\sigma(k) - n_\sigma(-k)]/n_\sigma^o$ where $n_\sigma^o = \max[n_\sigma(k)]$ denotes the maximum peak density of the momentum distribution in k -space. The two-photon detuning takes the different values of $\delta = \{-2.9, -1.9, 0.1, 1.1, 3.6\} \times E_r$ from top to bottom.

is switched off as described by gray curves. The lifetime for typical Raman coupling setting with a one-photon detuning $\Delta \sim 1.0$ GHz is about 40 ms that is mainly limited by single-photon scattering process. On the other hand, for the ^{173}Yb atoms a large one-photon detuning can be applied, in which case a much longer life time can be obtained.

When the Raman transition is at resonance $\delta \sim 0$, the $|m_F = \frac{5}{2}, \frac{3}{2}\rangle$ state is detuned by $\sim 2E_r$ from the $|m_F = \frac{1}{2}\rangle$ state. Such small detuning currently limits the effective spin- $\frac{1}{2}$ spin-orbit coupling in this system. Nevertheless, we experimentally confirm that the fractional population in the unwanted state $|m_F = \frac{1}{2}\rangle$ is smaller than 0.1 over the range of $\delta \gtrsim -1.0E_r$. Furthermore, the integrated momentum symmetry of $|\uparrow\rangle$ and $|\downarrow\rangle$ exhibits different behaviour for different values of δ as expected (see Fig. 4). As $\delta > 0$ becomes large where most of atoms are loaded into the $|\downarrow'\rangle$ state, the momentum asymmetry of $|\downarrow\rangle$ disappears after projection onto the bare state while $|\uparrow\rangle$ atoms show prominent momentum asymmetry due to spin-orbit coupling.

Discussion and Conclusion We have implemented SOC in a two-electron degenerate Fermi gas of ^{173}Yb atoms by using the Raman transition. The momentum distribution of the spin-orbit coupled Fermi gas exhibits strong asymmetry as a hallmark of SOC. The spin splitting is induced by AC stack shift, which can be precisely controllable by tuning light beam intensity. This avoids

applying magnetic field as in the experiments with alkali or lanthanide atoms, which suffers from magnetic field fluctuations. Furthermore, based on the present experiment a rich configuration, including spatially dependent two-photon detuning can be easily created by spatially dependent light strengths. Such configuration may create a spin texture in both momentum and position space. Finally, without the limit of fine structure splitting for excited levels, a longer life time can be obtained for SOC with ytterbium atoms when a large one-photon detuning is considered for the optical transitions. Being of many novel features in the ground manifold of hyperfine states, including the $SU(N)$ symmetry, the ytterbium fermions with laser induced SOC would open new possibilities to explore interesting new quantum physics.

APPENDIX

Experimental sequence

We first prepare a ultracold Fermi gas of ^{173}Yb atoms by trapping slow ytterbium atoms exiting from the Zeeman slower in the $^1\text{S}_0\text{-}^3\text{P}_1$ intercombination magneto-optical trap (MOT) at 556 nm [44]. The narrow linewidth $\Gamma = 2\pi \times 182$ kHz of the intercombination transition results low enough Doppler temperature allowing for cold gases around the temperature of $\sim 20\mu\text{K}$ in the MOT [45]. During the loading stage, however, the detuning of the MOT cooling light is externally modulated at a frequency of 100 kHz to increase the capture velocity of the intercombination MOT. The MOT cooling light at $I/I_{\text{sat}} = 90$ is detuned by 31Γ from the $^1\text{S}_0\text{-}^3\text{P}_1$ transition with the magnetic field gradient of 2.03 G/cm. Before the loading into the crossed optical dipole trap, we compress the MOT over 50 ms by increasing the magnetic field gradient to 11.6 G/cm and switching off the frequency modulation of the MOT light. Typically, we load $N \sim 3\text{-}4 \times 10^7$ atoms into the MOT within 20 s in this work.

The ytterbium atoms is then loaded into a 1064 nm crossed optical dipole trap (ODT) for forced evaporation with a trap depth up to $k_B \times 700 \mu\text{K}$ where k_B is the Boltzmann constant. The crossed optical trap consists of a tight ODT with 15 μm beam waist inclined at 15° from the horizontal plane and a horizontal shallow ODT with 56 μm beam waist. After the final stage of the optical evaporation, we achieve a six-component degenerate Fermi gas of $\sim 5.0 \times 10^4$ atoms at the temperature of $T/T_F < 0.35$ where T_F is the Fermi temperature of the trapped atom with the trapping frequency of $\bar{\omega} = 2\pi \times 130$ Hz.

After the evaporative cooling in the crossed ODT, a pair of Raman coupling beams is ramped up adiabatically with $\delta \simeq 10E_r$ as described in Fig. 5. Subsequently, the two-photon detuning of the Raman beam is exponentially tuned to a near-resonant frequency. To detect the momentum distribution of atoms, both Raman beams and the ODT beam are abruptly switched off before time-of-flight expansion followed by absorption imaging. The spin-sensitive blast beam is inserted for spin-sensitive imaging. Alternatively, the Optical Stern-Gerlach (OSG) light can be briefly pulsed after the magnetic bias field is rotated parallel to the OSG light within 200 ms. During the expansion, we apply 3 ms of 10 mW OSG light in order to separate the different spin components.

Calibration of differential AC stark shift

In contrast to alkali atoms, alkaline-earth-like atoms with two valence electrons have negligible linear and quadratic Zeeman shift. In alkali system, two hyperfine

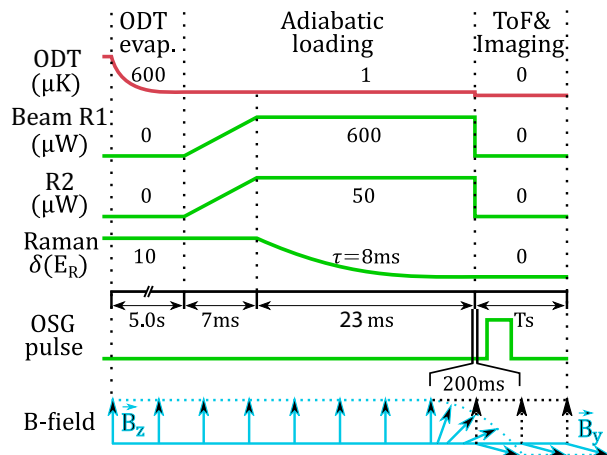


FIG. 5. (color online) Timing of the experimental sequence (details are available in text).

levels representing $|\uparrow\rangle$ and $|\downarrow\rangle$ are isolated from other states using quadratic Zeeman shift. In this work, we lift the hyperfine level in the ground manifold by introducing spin-dependent AC stark shift. The light shifts are given by the sum of the dipole matrix elements over the $^3\text{P}_1$ excited state manifold F , $\Delta E_{AC} = \sum_F \frac{|\Omega_{m_F, F}^q|^2}{\Delta_F}$

where $\Omega_{m_F, F}^q$ is the single-photon Rabi frequency of the ground-state $|m_F\rangle$ for the q polarized light and Δ_F is the single photon detuning with respect to the F excited hyperfine level. The differential AC stark shift between $|\uparrow, m_F = \frac{3}{2}\rangle$ and $|\downarrow, m_F = \frac{5}{2}\rangle$ is calibrated by monitoring the oscillation of the $|\uparrow\rangle$ ($|\downarrow\rangle$) population during the two-photon Rabi oscillation induced by a pair of co-propagating lights (see Fig. 6). In this case, no momentum is imparted to atoms so that the Rabi oscillation is momentum-insensitive, which allows for precise calibration. Furthermore, we set the intensity of the beam $R1$ to be much higher than beam $R2$ such that the differential AC stark shift is mainly tuned by the the beam $R1$.

In the three level Lambda system with a large single photon detuning, the excited states can be adiabatic eliminated. So the probability to perform a transition from initial purified state $|\downarrow, m_F = \frac{5}{2}\rangle$ to state $|\uparrow, m_F = \frac{3}{2}\rangle$ during a time τ is $P_{\uparrow}(\tau) = \frac{\Omega_{eff}^2}{\Omega_{eff}^2 + \delta^2/4} \sin^2(\sqrt{\Omega_{eff}^2 + \delta^2/4}\tau)$. Here, the effective Rabi frequency is $\Omega_{eff} = \sum_F \frac{\Omega_{\uparrow, F} \Omega_{\downarrow, F}}{\Delta_F}$, while the two photon detuning δ is decided by $\delta_{beat} - \delta_{AC}$. δ_{beat} is the beating frequency of the Raman coupling lasers, and δ_{AC} is the differential AC stark shift. In the experiment, we fix the effective Rabi frequency Ω_{eff} which only depends on the laser intensity and single photon detuning, so the differential AC stark shift keeps the same value in this process. Then we change the beating frequency and measure the modified Rabi frequency $\sqrt{\Omega_{eff}^2 + \delta^2/4}$ finding the res-

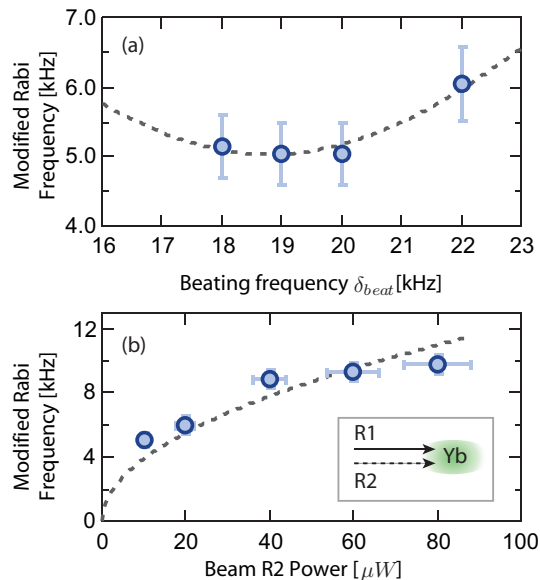


FIG. 6. (color online) Calibration of the differential AC Stark shift induced by the Raman light. The modified Rabi frequency is measured for different values of beating frequency δ_{beat} and the power of the beam R2 when the ytterbium atoms is exposed to a pair of co-propagating Raman beams.

onance condition of $\delta_{beat} = \delta_{AC}$ (see Fig. 6 (a)). In addition, the modified Rabi frequency is monitored for different values of Ω_{eff} which is complementary calibration of the differential AC Stark shift in the system as shown in Fig. 6 (b).

ACKNOWLEDGEMENT

G.-B. J. acknowledges the generous support from the Hong Kong Research Grants Council and the Croucher Foundation through ECS26300014, GRF16300215 and the Croucher Innovation grants respectively. X.-J. L. also thanks the support from MOST (Grant No. 2016YFA0301600) and NSFC (No. 11574008).

* Present address: Guangdong Provincial Key Laboratory of Quantum Engineering and Quantum Materials, School of Physics and Telecommunication Engineering, South China Normal University, Guangzhou, China.

- [1] I. Bloch and W. Zwerger, *Reviews of Modern Physics* **80**, 885 (2008).
- [2] J. Dalibard, F. Gerbier, G. Juzeliūnas, and P. Oehberg, *Reviews of Modern Physics* **83**, (2011).
- [3] H. Zhai, *Reports on Progress in Physics* **78**, 026001 (2015).
- [4] N. Nagaosa, J. Sinova, S. Onoda, A. H. MacDonald, and N. P. Ong, *Reviews of Modern Physics* **82**, 1539 (2010).

- [5] M. Hasan and C. Kane, *Reviews of Modern Physics* **82**, 3045 (2010).
- [6] X. L. Qi and S. C. Zhang, *Reviews of Modern Physics* (2011).
- [7] Y. J. Lin, K. Jiménez-García, and I. B. Spielman, *Nature* **471**, 83 (2011).
- [8] J. Higbie and D. M. Stamper-Kurn, *Physical Review Letters* **88**, 090401 (2002).
- [9] X.-J. Liu, M. Borunda, X. Liu, and J. Sinova, *Physical Review Letters* **102** (2009).
- [10] I. B. Spielman, *Physical Review A* **79**, 063613 (2009).
- [11] X. Luo, L. Wu, J. Chen, Q. Guan, K. Gao, Z.-F. Xu, L. You, and R. Wang, *Scientific reports* **6**, 18983 (2016).
- [12] K. Jiménez-García, L. J. LeBlanc, R. A. Williams, M. C. Beeler, C. Qu, M. Gong, C. Zhang, and I. B. Spielman, *Phys. Rev. Lett.* **114**, 125301 (2015).
- [13] R. A. Williams, L. J. LeBlanc, K. Jiménez-García, M. C. Beeler, A. R. Perry, W. D. Phillips, and I. B. Spielman, *Science* **335**, 314 (2012).
- [14] J.-Y. Zhang, S.-C. Ji, Z. Chen, L. Zhang, Z.-D. Du, B. Yan, G.-S. Pan, B. Zhao, Y.-J. Deng, H. Zhai, S. Chen, and J.-W. Pan, *Phys. Rev. Lett.* **109**, 115301 (2012).
- [15] C. Qu, C. Hamner, M. Gong, C. Zhang, and P. Engels, *Phys. Rev. A* **88**, 021604 (2013).
- [16] C. Hamner, C. Qu, Y. Zhang, J. Chang, M. Gong, C. Zhang, and P. Engels, *Nat Commun* **5**, (2014).
- [17] S.-C. Ji, J.-Y. Zhang, L. Zhang, Z.-D. Du, W. Zheng, Y.-J. Deng, H. Zhai, S. Chen, and J.-W. Pan, *Nat Phys* **10**, 314 (2014).
- [18] A. J. Olson, S.-J. Wang, R. J. Niffenegger, C.-H. Li, C. H. Greene, and Y. P. Chen, *Phys. Rev. A* **90**, 013616 (2014).
- [19] S.-C. Ji, L. Zhang, X.-T. Xu, Z. Wu, Y. Deng, S. Chen, and J.-W. Pan, *Phys. Rev. Lett.* **114**, 105301 (2015).
- [20] R. A. Williams, M. C. Beeler, L. J. LeBlanc, K. Jiménez-García, and I. B. Spielman, *Phys. Rev. Lett.* **111**, 095301 (2013).
- [21] Z. Fu, L. Huang, Z. Meng, P. Wang, L. Zhang, S. Zhang, H. Zhai, P. Zhang, and J. Zhang, *Nat Phys* **10**, 110 (2014).
- [22] P. Wang, Z.-Q. Yu, Z. Fu, J. Miao, L. Huang, S. Chai, H. Zhai, and J. Zhang, *Physical Review Letters* **109**, 095301 (2012).
- [23] L. W. Cheuk, A. T. Sommer, Z. Hadzibabic, T. Yefsah, W. S. Bakr, and M. W. Zwierlein, *Physical Review Letters* **109**, 095302 (2012).
- [24] N. Q. Burdick, Y. Tang, and B. L. Lev, *arXiv.org*, arXiv:1605.03211 (2016), 1605.03211.
- [25] Z. Wu, L. Zhang, W. Sun, X.-T. Xu, B.-Z. Wang, S.-C. Ji, Y. Deng, S. Chen, X.-J. Liu, and J.-W. Pan, *arXiv.org*, arXiv:1511.08170 (2015), 1511.08170.
- [26] L. Huang, Z. Meng, P. Wang, P. Peng, S.-L. Zhang, L. Chen, D. Li, Q. Zhou, and J. Zhang, *Nat Phys* **12**, 540 (2016).
- [27] X. Cui, B. Lian, T.-L. Ho, B. L. Lev, and H. Zhai, *Phys. Rev. A* **88**, 011601 (2013).
- [28] M. L. Wall, A. P. Koller, S. Li, X. Zhang, N. R. Cooper, J. Ye, and A. M. Rey, *Phys. Rev. Lett.* **116**, 035301 (2016).
- [29] J. Li, W. Huang, B. Shteynas, S. Burchesky, F. C. Top, E. Su, J. Lee, A. O. Jamison, and W. Ketterle, (2016), 1606.03514.
- [30] A. J. Daley, *Quantum Information Processing* **10**, 865 (2011).

- [31] M. A. Cazalilla and A. M. Rey, Reports on Progress in Physics **77**, 124401 (2014).
- [32] G. Pagano, M. Mancini, G. Cappellini, P. Lombardi, F. Schäfer, H. Hu, X.-J. Liu, J. Catani, C. Sias, M. Inguscio, and L. Fallani, Nature Physics **10**, 198 (2014).
- [33] S. Taie, R. Yamazaki, S. Sugawa, and Y. Takahashi, Nat.Phys **8**, 825 (2012).
- [34] M. Mancini, G. Pagano, G. Cappellini, L. Livi, M. Rider, J. Catani, C. Sias, P. Zoller, M. Inguscio, M. Dalmonte, and L. Fallani, Science **349**, 1510 (2015).
- [35] S. Nakajima, T. Tomita, S. Taie, T. Ichinose, H. Ozawa, L. Wang, M. Troyer, and Y. Takahashi, Nat.Phys **12**, 296 (2016).
- [36] D. L. Campbell, R. M. Price, A. Putra, A. Valdés-Curiel, D. Trypogeorgos, and I. B. Spielman, Nature Communications **7**, 10897 (2016).
- [37] S. Barbarino, L. Taddia, D. Rossini, L. Mazza, and R. Fazio, Nature Communications **6**, 8134 (2015).
- [38] D. Banerjee, M. Bögli, M. Dalmonte, E. Rico, P. Stebler, U. J. Wiese, and P. Zoller, Physical Review Letters **110**, 125303 (2013).
- [39] Y. T. Nathaniel Q. Burdick and B. L. Lev, arXiv:1605.03211 (2016).
- [40] S. Stellmer, R. Grimm, and F. SCHRECK, Physical Review A **84**, 043611 (2011).
- [41] S. Taie, Y. Takasu, S. Sugawa, R. Yamazaki, T. Tsujimoto, R. Murakami, and Y. Takahashi, Physical Review Letters **105**, 190401 (2010).
- [42] C. Cohen-Tannoudji, J. Dupont-Roc, and G. GRYNBERG, *Atom-Photon Interactions* (Wiley, New York, 1992).
- [43] P. Wang, Z.-Q. Yu, Z. Fu, J. Miao, L. Huang, S. Chai, H. Zhai, and J. Zhang, Phys. Rev. Lett. **109**, 095301 (2012).
- [44] T. Fukuhara, Y. Takasu, M. Kumakura, and Y. Takahashi, Physical Review Letters **98**, 030401 (2007).
- [45] T. Kuwamoto, K. Honda, Y. Takahashi, and T. Yabuzaki, Physical Review A **60**, R745 (1999).